Full-Wave Fast Solver for Circuit Devices Modeling

Yuteng Zheng, Yanwen Zhao, Zaiping Nie, and Qiangming Cai

Department of Electrical Engineering
University of Electronic Science and Technology of China, Chengdu, 611731, China
zhengyuteng413@gmail.com, ywzhao@uestc.edu.cn

Abstract ─ The analysis of complex circuit components with electrically small size is an important problem for radio frequency circuit modeling. In this paper, we present a fast solver which is based on low-frequency stable integral equation and accelerated with the multilevel accelerated Cartesian expansion algorithm (MLACEA). MLACE algorithm is usually based on electric field integral equation which suffers from low-frequency breakdown problems. To keep the algorithm stable, the augmented electric field integral equation (AEFIE) is used in our solver. Regarding the truncation order of the expansion, the efficiency and accuracy of MLACEA are investigated. By adjusting the truncation order, we can keep the algorithm in good performance. Numerical examples show the efficiency and the capability of the proposed method.

Index Terms ─ Fast algorithm, low-frequency problem, method of moments.

I. INTRODUCTION

The electric field integral equation (EFIE) solved by the method of moments (MoM) [4] is widely used in practical RF and microwave circuit modeling and design [6]. Due to the increasing integration density, the electromagnetic (EM) analysis of circuit problems become more challenging. Furthermore, the manufacturing technique of three-dimensional (3D) passives RF components [1], logic cells [2] and system in package (SIP) techniques [3] have received considerable amount of attention recently. By utilizing these techniques, the 2D planar structures are changed into 3D multilayer stereoscopic and even curved structures. Because of the increasing complexity, the scale of numerical problem for EM modeling is dramatically increased.

For 3D circuit modeling, the following two problems need to be concerned. One is the high computational complexity of MoM. To reduce the complexity and accelerated the simulation speed, many kinds of fast algorithms have been studied. The algorithms based on fast Fourier transforms (FFT) are widely used for quasi-planar structures. Suppose the scale of a problem is N. Then numerical complexity of the matrix vector production (MVP) and memory consumption can be reduced from $O(N^2)$ to $O(N \log N)$ [5,6]. However, FFT methods require a projection between the original mesh and the uniform grid, so it is difficult to balance the workload for multiscale problems. The oct-tree based fast algorithms, such as the low-frequency multilevel fast multipole algorithm (LF-MLFMA) [7] and the multilevel accelerated Cartesian expansion algorithm (MLACEA) [8,9], have lower numerical complexity. Even for 3D structures the MVP time and memory consumptions of these two methods have $O(N)$ complexity. LF-MLFMA has been successfully applied on low-frequency EM modeling such as [7,10], while the implementation of MLACEA on low-frequency EM modeling is seldom reported.

The other problem need to be concerned is the low-frequency breakdown problem of EFIE, which restricts the fast algorithm to handle low-frequency EM problems. The low-frequency breakdown problem of EFIE occurs when the discretization is so fine that the mesh size is much smaller than the wavelength [11]. In this situation, the condition number of the matrix increases, and the convergence of iterative method is getting worse. The low-frequency breakdown problem often influenced the accuracy of circuit device modeling. Loop-tree decomposition [12] is usually employed to remedy the low-frequency breakdown problem, and many fast solvers base on this method have been developed [6,7]. However, searching for loop basis functions is difficult for multiple connected surfaces, especially in 3D case. Recently some low-frequency stable EFIE methods were developed, such as the augmented electric field integral equations (AEFIE) [10], the current and charge integral equations (CCIE) [13], the separated potential integral equations (SPIE) [14], and surface integral equations using constraint-based Helmholtz decompositions [16,17]. They all remedy the low-frequency breakdown problem successfully.

In this paper, we used AEFIE to remedy the low-frequency breakdown problem. Compared with other integral equations, the operator in AEFIE is simpler. This advantage not only results in simplicity of programming

but also in less memory and time consumption of the fast algorithm. However, the AEFIE still suffers from the low-frequency inaccuracy problem in extremely low-frequency, but this inaccuracy problem can be eliminated with perturbation method [15]. The paper is organized as follows. The AEFIE and its MoM solution are reviewed in Section II. Then, in order to remedy the low-frequency breakdown problem of EFIE and to keep the matrix equation in good condition, the AEFIE is used as the basic formula of the MLACEA algorithm. Particularly, the truncation order of MLACEA is analyzed to figure out its influence on the efficiency and the accuracy. At last, several large unknown targets have been simulated to show the capability of the proposed method.

II. THEORY

A. Augmented electric field integral equation

Consider a perfect electric conducting (PEC) surface S placed in free space is excited by a incident field $\boldsymbol{E}^{inc}$. The mixed potential integral equation in terms of the induced current $\boldsymbol{J}(\boldsymbol{r})$ on the PEC surface S can be achieved by using the tangential boundary condition of electric field, given as:

$$
\begin{cases}
\boldsymbol{n} \times \boldsymbol{E}^{inc}(\boldsymbol{r}) = \boldsymbol{n} \times \left[j\omega \boldsymbol{A}(\boldsymbol{r}) + \nabla \Phi(\boldsymbol{r}) \right] \\
\boldsymbol{A}(\boldsymbol{r}) = \mu \int_S \mathrm{d}S' \, \boldsymbol{J}(\boldsymbol{r}') G(\boldsymbol{r}, \boldsymbol{r}') \\
\Phi(\boldsymbol{r}) = j\eta k^{-1} \int_S \mathrm{d}S' \, \nabla' \cdot \boldsymbol{J}(\boldsymbol{r}') G(\boldsymbol{r}, \boldsymbol{r}')
\end{cases}
\tag{1}
$$

In the above equations, $G(\boldsymbol{r}, \boldsymbol{r}')$ is the scalar Green's function in free space:

$$
G(\boldsymbol{r}, \boldsymbol{r}') = \frac{\mathrm{e}^{-jkR}}{4\pi R},
\tag{2}
$$

where $R = |\boldsymbol{r} - \boldsymbol{r}'|$ represents the distance between the source point $\boldsymbol{r}'$ and the field point $\boldsymbol{r}$. $\eta = \sqrt{\mu_0/\varepsilon_0}$ denotes the wave impendence, $k = \omega\sqrt{\varepsilon_0\mu_0}$ denotes the wave number of free space and $\boldsymbol{n}$ is the unit outer normal to surface S. This integral equation suffers from the low-frequency breakdown problem, because of the different frequency dependence of vector potential and scalar potential in the low-frequency region [11]. In order to separate the vector and scalar potential and remove the frequency dependence, the current continuity equation given as:

$$
\nabla \cdot \boldsymbol{J}(\boldsymbol{r}) = -j\omega \rho(\boldsymbol{r}),
\tag{3}
$$

is added. It works as a constraint for the charge and the current. To get the discretized form of the equations, the surface current $\boldsymbol{J}(\boldsymbol{r})$ is expanded over a set of RWG basis functions as:

$$
\boldsymbol{f}_n(\boldsymbol{r}) = \begin{cases}
(\boldsymbol{r} - \boldsymbol{r}_n^+)/(2A_n^+), & \boldsymbol{r} \in T_n^+ \\
-(\boldsymbol{r} - \boldsymbol{r}_n^-)/(2A_n^-), & \boldsymbol{r} \in T_n^-
\end{cases}.
\tag{4}
$$

The charge is expanded as pulse functions:

$$
h_n(\boldsymbol{r}) = 1/A_n, \quad \boldsymbol{r} \in T_n,
\tag{5}
$$

where A_i is the area of triangle T_i. Then EFIE is tested by RWG basis functions $\boldsymbol{f}_m(\boldsymbol{r})$, and the current continuity equation is tested by $h_m(\boldsymbol{r})$. Matrix equations can be finally written as:

$$
\boldsymbol{B} \cdot jk\boldsymbol{I} + \boldsymbol{D}^T \cdot \boldsymbol{P} \cdot c\boldsymbol{\rho} = \eta^{-1}\boldsymbol{b},
\tag{6a}
$$

$$
\boldsymbol{D} \cdot jk\boldsymbol{I} + \tilde{\boldsymbol{I}} \cdot ck^2 \boldsymbol{\rho} = \boldsymbol{0}.
\tag{6b}
$$

The elements of sub matrices are defined as:

$$
b(m) = \int_{S_m} \mathrm{d}S \, \boldsymbol{f}_m(\boldsymbol{r}) \cdot \boldsymbol{E}^{inc}(\boldsymbol{r}),
\tag{7}
$$

$$
B(m,n) = \int_{S_m} \mathrm{d}S \, \boldsymbol{f}_m(\boldsymbol{r}) \cdot \int_{S_n} \mathrm{d}S' \, \boldsymbol{f}_n(\boldsymbol{r}') G(\boldsymbol{r}, \boldsymbol{r}'),
\tag{8}
$$

$$
P(m,n) = \int_{T_m} \mathrm{d}S \, h_m(\boldsymbol{r}) \int_{T_n} \mathrm{d}S' \, h_n(\boldsymbol{r}') G(\boldsymbol{r}, \boldsymbol{r}'),
\tag{9}
$$

$$
D(m,n) = \frac{1}{A_n} \int_{T_m} \mathrm{d}S \, h_m(\boldsymbol{r}) \nabla \cdot \boldsymbol{f}_n(\boldsymbol{r}),
\tag{10}
$$

where $S_n = T_n^+ \bigcup T_n^-$. $\boldsymbol{I}$ and $\boldsymbol{\rho}$ denote the coefficients of current and charge unknowns. $\tilde{\boldsymbol{I}}$ is the identity matrix. c is the light speed in free space. In this matrix equation, the vector potential and scalar potential are balanced. After using a proper frequency scaling [10], the low-frequency breakdown can be remedied.

B. Implementation of MLACEA

In this section, MLACEA is applied on the AEFIE for acceleration. Similar to MLFMA, the basis functions are divided into groups of small cubes using the oct-tree structure. Based on whether two boxes are within one box interval, the interaction between the basis functions and the testing functions inside any two boxes is classified as the near-field interaction or the far-field interaction.

To calculate the far-field interaction with MLACEA, the scalar Green's function is expanded with the Cartesian tensor expansion which is given as:

$$
\psi(\boldsymbol{r} - \boldsymbol{r}') = \sum_{q=0}^{\infty} \frac{(-1)^q}{q!} \boldsymbol{r}'^{(q)} \cdot q \cdot \nabla^{(q)} \psi(\boldsymbol{r}),
\tag{11}
$$

where $\nabla^{(q)}$ is q-fold grid operator of $\boldsymbol{r}$ and $\boldsymbol{A}^{(p+q)} \cdot q \cdot \boldsymbol{B}^{(q)}$ represents q-fold tensor contraction between tensors $\boldsymbol{A}^{(p+q)}$ and $\boldsymbol{B}^{(q)}$. Then this expansion is applied on the Green's function. As an example, the scalar Green's function is expanded with two-level accelerated Cartesian expansion algorithm in the following derivation. For far-field group interaction, the scalar Green's function $G(\boldsymbol{r}, \boldsymbol{r}')$ is expanded using (11) twice, both in the center of source group $\boldsymbol{r}_\alpha^c$ and the center of field group $\boldsymbol{r}_{\alpha'}^c$ as:

$$
G(\boldsymbol{r}, \boldsymbol{r}') \approx \sum_{q=0}^{Q} \frac{1}{q!} (\boldsymbol{r} - \boldsymbol{r}_\alpha^c)^{(q)} \cdot q \cdot \sum_{p=0}^{Q} \nabla^{(p+q)} G(\boldsymbol{r}_\alpha^c, \boldsymbol{r}_{\alpha'}^c)
$$
$$
\cdot p \cdot \left[\frac{(-1)^p}{p!} (\boldsymbol{r}' - \boldsymbol{r}_{\alpha'}^c)^{(p)} \right],
\tag{12}
$$

where Q is the truncation order.

Then we can apply this expansion in MoM. When we solve the MoM linear equations using an iterative method, the matrix vector product (MVP) is a very time consuming part. To reduce the MVP time, fast algorithm is applied. The matrices in (6b) are calculated directly because they are highly sparse matrix. While MLACEA is applied on the matrices in (6a) to speed up the calculation. After the expansion using (12), the storage for far-field interaction matrix is no more needed, and the calculation of:

$$V = B \cdot jkI + D^T \cdot P \cdot c\rho, \quad (13)$$

can be represented by MLACEA approximately, given as:

$$V \approx B_{near} \cdot jkI + D^T \cdot P_{near} \cdot c\rho + jkV_A^{far} + cV_\Phi^{far}, \quad (14)$$

where B_{near} and P_{near} represent the near-field interactions corresponding to vector and scalar potentials respectively. They are computed and stored using conventional MoM. V_A^{far} and V_Φ^{far} are far-field interactions of vector potential and scalar potential. Corresponding to any testing function $f_m(r)$ or $h_n(r)$, we denote the contributions from charge and current in far-field groups as $V_A^{far}(m)$ or $V_\Phi^{far}(m)$. They can be represented into two level MLACEA form as:

$$V_A^{far}(m) = \sum_{q=0}^{Q} F_m^{A,-}(q,r_\alpha^c) \cdot q \cdot$$
$$\sum_{p=0}^{Q} \sum_{\alpha' \in G_\alpha^{far}} T(q+p;r_\alpha^c,r_{\alpha'}^c) \cdot p \cdot S_{\alpha'}^A(p,r_{\alpha'}^c), \quad (15a)$$

$$V_\Phi^{far}(m) = \sum_{q=0}^{Q} F_m^{\Phi,-}(q,r_\alpha^c) \cdot q \cdot$$
$$\sum_{p=0}^{Q} \sum_{\alpha' \in G_\alpha^{far}} T(q+p;r_\alpha^c,r_{\alpha'}^c) \cdot p \cdot S_{\alpha'}^\Phi(p,r_{\alpha'}^c), \quad (15b)$$

where G_α^{far} denotes the set of far-field groups related to the group α. In MLACEA, the tensors formed by aggregating the source points inside a group are called multipole expansions. The corresponding current and charge multipole expansions are given as:

$$S_{\alpha'}^A(p,r_{\alpha'}^c) = \sum_{n \in G_{\alpha'}^{self}} I_n F_n^{A,+}(p,r_{\alpha'}^c), \quad (16a)$$

and

$$S_{\alpha'}^\Phi(p,r_{\alpha'}^c) = \sum_{n \in G_{\alpha'}^{self}} \rho_n F_n^{\Phi,+}(p,r_{\alpha'}^c), \quad (16b)$$

where $G_{\alpha'}^{self}$ represents the set of current and charge basis functions in the group α'. $F_n^{A,+}$ and $F_n^{\Phi,+}$ are aggregation factors corresponding to each basis function, called multipole factors. The multipole factors of currents and charges in (16) are given ast:

$$F_n^{A,+}(p,r_{\alpha'}^c) = \frac{(-1)^p}{p!} \int_{S_n} dS' \; (r'-r_{\alpha'}^c)^{(p)} f_n(r'), \quad (17a)$$

and

$$F_n^{\Phi,+}(p,r_{\alpha'}^c) = \frac{(-1)^p}{p!} \int_{T_n} dS' \; (r'-r_{\alpha'}^c)^{(p)} h_n(r'). \quad (17a)$$

The integration regions of the two integrals above are different. One is on a basis function, and the other is on a triangle patch. The interaction from source group to field group is connected by the translation operator:

$$T(p;r_\alpha^c,r_{\alpha'}^c) = \nabla^{(p)} G(r_\alpha^c,r_{\alpha'}^c). \quad (18)$$

It is applied on the multipole expansion and transforms them into the local expansion $R_\alpha(q,r_\alpha^c)$ in field region. Then the local expansion will be contracted with the local factors to achieve $V_A^{far}(m)$ and $V_\Phi^{far}(m)$. The local factors in (15) are:

$$F_m^{A,-}(p,r_\alpha^c) = \frac{1}{p!} \int_{S_m} dS \; (r-r_\alpha^c)^{(p)} f_m(r), \quad (19a)$$

$$F_m^{\Phi,-}(p,r_\alpha^c) = \frac{1}{p!} \int_{S_m} dS \; (r-r_\alpha^c)^{(p)} \nabla \cdot f_m(r). \quad (19b)$$

Similarly the multilevel form use a translation operator between the parent level and the child level recursively. With multilevel recursion, higher efficiency can be achieved. Here, (15a) which corresponds to the vector potential is used as an example to show the derivation of the multilevel algorithm. It is written in a new form as:

$$V_A^{far}(m) = \sum_{p=0}^{Q} F_m^{A,-}(p,r_{\alpha_l}^c) \cdot p \cdot \left[R_{\alpha_l}^l(p,r_{\alpha_l}^c) \right.$$
$$\left. + \sum_{p=0}^{Q} \sum_{\alpha_l' \in G_{\alpha_l}^{rel}} T(q+p;r_{\alpha_l}^c,r_{\alpha_l'}^c) \cdot p \cdot S_{\alpha_l'}^A(p,r_{\alpha_l'}^c) \right], \quad (20)$$

where $R_{\alpha_l}^l(q,r_{\alpha_l}^c)$ is the local expansion of α_l on the l th level. $G_{\alpha_l}^{rel}$ indicates the set of the distant relative groups. The term α_{l-1} indicates the parent group of α_l, and the distant relative groups can be defined as the groups on the l th level who are not only in the far-field region of α_l but also inside the near-field region of α_{l-1}. On each level, the local expansion is given as:

$$R_{\alpha_l}^l(p,r_{\alpha_l}^c) = \sum_{q=p}^{Q} \frac{1}{(q-p)!} R_{\alpha_{l-1}}^{l-1}(q,r_{\alpha_{l-1}}^c)$$
$$\cdot (q-p) \cdot (r_{\alpha_l}^c - r_{\alpha_{l-1}}^c)^{(q-p)} \quad (21)$$
$$+ \sum_{p=0}^{Q} \sum_{\alpha_l' \in G_{\alpha_l}^{rel}} T(q+p;r_{\alpha_l}^c,r_{\alpha_l'}^c) \cdot p \cdot S_{\alpha_l'}^A(p,r_{\alpha_l'}^c),$$

where $r_{\alpha_l}^c$ and $r_{\alpha_{l-1}}^c$ are the centroids of the child groups and the parent group respectively. The first part on the

right hand side of this equation does not need to be calculated when this equation is applied on the highest level. Similarly, the multipole-to-multipole translation is expressed with:

$$S_{\alpha'}^{l-1}(p, \boldsymbol{r}_{\alpha_{l-1}}^c) = \sum_{\alpha_l' \in G_{\alpha_{l-1}'}^{son}} \sum_{q=p}^{Q} \frac{1}{(q-p)!} S_{\alpha'}^l(q, \boldsymbol{r}_{\alpha_l}^c) \qquad (22)$$
$$(\boldsymbol{r}_{\alpha_{l-1}}^c - \boldsymbol{r}_{\alpha_l'}^c)^{(q-p)},$$

where $G_{\alpha_{l-1}'}^{son}$ indicates the child groups of α_{l-1}'. This equation is applied on the aggregation of child groups. Recursively using (21) and (22), the algorithm can be easily applied to multilevel form.

III. NUMERICAL RESULTS

All numerical computations have been performed on a 64-bit PC using Intel core-i5 CPU with 3.0 GHz clock speed. The generalized minimum residual (GMRES) which restarts every 30 iterations was used as solver of linear equation.

The computational complexity of proposed method is analyzed in the first example. A PEC cube with a side length of 10 mm is calculated at 300 MHz. The target is divided into 1200 triangular patches, and the induced current is then expanded with 1800 RWG basis functions. By connecting each pair of the adjacent midpoints of the three edges in a triangular patch, this triangle is divided into the four small triangular patches with one-half of the original edge length. This refinement is done recursively to obtain five different discretization schemes. They are named from coarse to fine by the letters A to F. The group size is optimized to keep the average number of unknowns around 30 approximately in each group on the bottom level. The truncation order of Cartesian expansion is set as 2. The CPU times for calculating the near-field matrix and the matrix vector product are both shown in Fig. 1. The black solid line, a linear function in terms of the number of unknowns N, is shown as a reference. According to this solid line, it is easy to find out that the memory consumption, the CPU time for the near-field matrix calculation and the MVP are all $O(N)$.

The error convergence of MLACEA when calculating the finest mesh F is discussed. The mesh contains 1228800 triangle patches and 1843200 RWG basis functions. For the Cartesian expansion the truncation order Q impacts the accuracy of the algorithm. To balance the efficiency and accuracy, the truncation order should be carefully selected. Although the numerical precision has been tested in previous work by calculating the relative error of the scalar potential, here we evaluate the relative error of the impedance matrix so that the error induced by the transformation form potential to impedance matrix elements can be included. The relative error defined as:

$$O(\boldsymbol{Z}) = \frac{\|\delta \boldsymbol{V}\|_2}{\|\boldsymbol{V}\|_2} = \frac{\|V_{ACE}(\boldsymbol{Z}, \boldsymbol{I}) - \boldsymbol{Z}_{MoM} \cdot \boldsymbol{I}\|_2}{\|\boldsymbol{Z}_{MoM} \cdot \boldsymbol{I}\|_2}, \qquad (23)$$

is used to measure the truncation error of the algorithm quantitatively. By a given vector $\boldsymbol{I}$, $\boldsymbol{Z}_{MoM} \cdot \boldsymbol{I}$ is calculated by direct multiplication. $V_{ACE}(\boldsymbol{Z}, \boldsymbol{I})$ is achieved by MLACEA. In Table 1, as truncation order increases, the time consumption of MVP grows exponentially, while the relative error only decreases slowly. After the trade-off between efficiency and accuracy, two orders expansion is used in the following example for better numerical performances. With the help of the preconditioner in [10], the residual error can be converged to less than 10^{-4} within 110 iterations. The details on the convergence history of five cases are shown in Fig. 2. The bi-static RCS results of first five cases, shown in Fig. 3, are in good agreement.
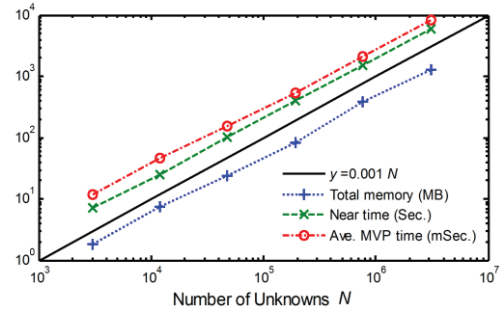
Fig. 1. The computational complexity of time and memory for the proposed method.

Table 1: Relative error convergence and normalized time consumption

Truncation Order	Normalized Time	Relative Error $O(B)$	Relative Error $O(P)$
0	1	1.92×10^{-1}	1.08×10^{-1}
1	2	3.98×10^{-2}	2.13×10^{-2}
2	5	9.76×10^{-3}	5.71×10^{-3}
3	16	2.98×10^{-3}	1.76×10^{-3}
4	44	1.06×10^{-3}	5.36×10^{-4}
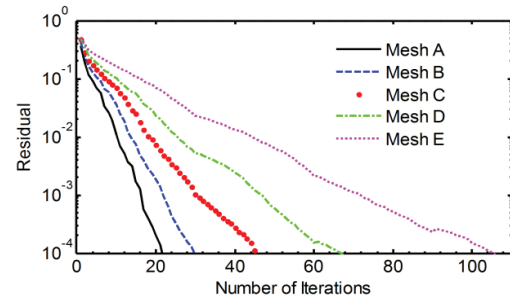
Fig. 2. History of iteration for different mesh densities.
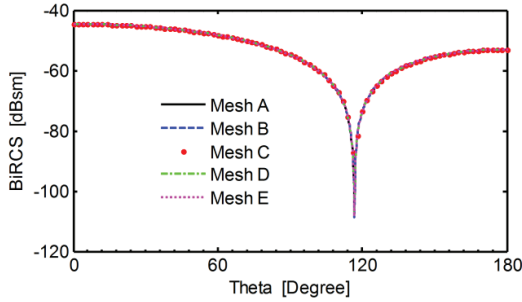
Fig. 3. The bi-static RCS results for different mesh densities.

In the second example, a 3D micro-coil inductors has been modeled to test the capability of the algorithm. The design of the inductor is referred from [1], with the length of 275 μm, the width of 75 μm, the height of 100 μm, the inner diameter of 50 μm, and the total length of about 5.25 mm. Because the low-frequency breakdown problem is more serious compared with lossy media, the inductor is set as a PEC to investigate the performance of our solver. The inductor model is divided into 6776 triangles. Based on these triangles, 8862 current unknowns and 6776 charge unknowns are formed. Port 1 is excited with delta gap voltage source as shown in Fig. 4. To verify the accuracy of the solution, the inductance is extracted by the three methods, namely: EFIE, AEFIE and AEFIE combined with MLACEA. They are compared through a wide frequency band from 500 MHz to 25 GHz. The structure is divided into 5 levels oct-tree to keep the average number of unknowns in each group within 20 RWG basis functions. The truncation order is set as two to cut down the time consumption. EFIE is solved by LU decomposition for its bad condition number of matrix in the low-frequency. AEFIE is solved by GMRES both with and without the acceleration of MLACEA. The comparison of consumption in computation from Table 2 proves that AEFIE combined with MLACEA is much more efficient than the direct MoM solver. The results of inductance obtained by AEFIE combined with MLACEA have the same the accuracy as the traditional MoM throughout the whole bandwidth. On the other hand, EFIE can't provide the correct inductance results in the low-frequency band from 500 MHz to 8 GHz due to the low-frequency breakdown of the solutions.

Next, six discretizations of a spiral inductor are generated and named as A to F, from coarse to fine. Mesh A has 6147 inner edges. While F has 285 909 edges, which is 44 times larger than A. The total size of the inductor is 1.2×10^{-3} λ at 3 GHz. Figure 5 shows the extracted inductance for all the cases. The inductance converges to 2.348 nH as the mesh density increases. It

agrees well with the result from the MoM. With the limit of computer memory, mesh A is calculated using the MoM and the inductance is 2.329 nH. The surface current distribution on the densest mesh F is presented in Fig. 6 with color bar in dB scale. The computational costs of mesh E and F are summarized in Table 3 in detail. By keeping the average number of unknowns in each finest box around 20, the fast solver consumed very little time in near-field matrix calculation. All cases can converge to 10^{-4} quickly and show good stability.
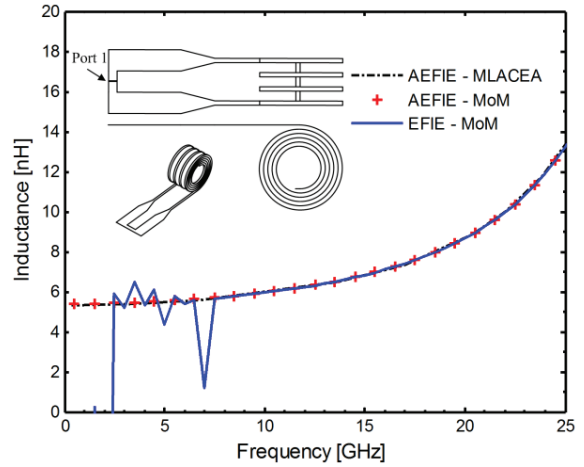
Fig. 4. The inductor model and the inductance calculated by EFIE-MoM, AEFIE-MoM and AEFIE-MoM with MLACEA acceleration.

Table 2: Average memory and time consumption of one frequency point using AEFIE

	MoM	MLACEA
Total memory (MB)	1960	59
Near field calculation time (s)	160	3.8
Number of iterations	48	49
Time per iteration (s)	1.05	0.12
Total time (s)	210	10
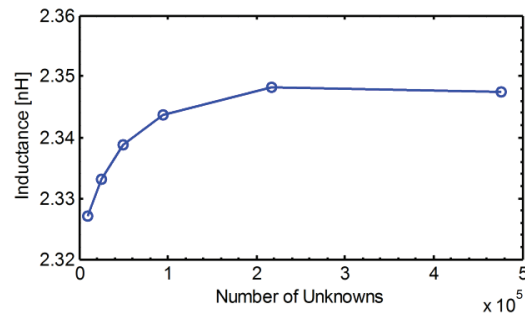
Fig. 5. The inductance calculated by meshes in different densities.
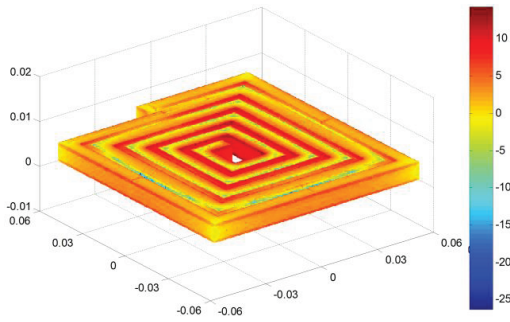
Fig. 6. The current distribution of inductor model: mesh F, unit in mm.

Table 3: Memory and time consumption of different mesh density

	Mesh E	Mesh F
Number of total unknowns	217 270	476 515
Total memory (MB)	813	1 239
Near field calculation time (s)	146	233
Number of iterations	149	188
Time per iteration (s)	1.23	2.59
Total iteration time (s)	184	502
Total time (s)	334	747

IV. CONCLUSION

A fast numerical algorithm, AEFIE combined with MLACEA, has been presented in this paper to model the circuit devices with electrically small and complex structures. The condition number of the impedance matrix is greatly improved by AEFIE. Because of this MLACEA shows a good stability for the low-frequency problems with large number of unknowns. With the optimization of the truncation order, the efficiency as well as the accuracy of the solver has been ensured. Its ability to cut down the memory cost and CPU time consumption can be put to use. Some work are under going to eliminate the low-frequency inaccuracy problem of AEFIE, in order to achieve a stable solver for more wide frequency band.

ACKNOWLEDGMENT

REFERENCES

[1] M. S. Mohamed Ali, B. Bycraft, C. Schlosser, B. Assadsangabi, and K. Takahata, "An out-of-plane spiral-coil inductor formed using locally controlled bimorph actuation," *Micro. Nano Lett.*, vol. 6, pp. 1016-1018, Dec. 2011.

[2] S. J. Kim, J. J. Lee, H. J. Kang, J. B. Choi, Y-S. Yu, Y. Takahashi, and D. G. Hasko, "One electron-based smallest flexible logic cell," *Appl. Phys. Lett.*, vol. 101, 183101, 2012.

[3] S. F. Al-Sarawi, D. Abbott, and P. D. Franzon, "A review of 3D packaging technology," *IEEE Trans. CPMT*, vol. 21. pp. 2-14, Jan. 1998.

[4] R. F. Harrington, *Field Computation by Moment Methods*, IEEE Press, New York, 1993.

[5] S. M. See and J-F. Lee, "A fast IE-FFT algorithm for solving PEC scattering problems," *IEEE Tram. Magn.*, vol. 41, pp. 1476-1479, May 2005.

[6] V. I. Okhmatovski, J. Morsey, and A. C. Cangellaris, "Loop-tree implementation of the adaptive integral method (AIM) for numerically-stable, broadband, fast electromagnetic modeling," *IEEE Trans. Antennas Propagat.*, vol. 52, pp. 2130-2140, Aug. 2004.

[7] J. S. Zhao and W. C. Chew. "Applying LF-MLFMA to solve complex PEC structures," *Micro. Opt. Technol. Lett.*, vol. 28, pp. 155-160, Feb. 2001.

[8] B. Shanker and H. Huang, "Accelerated Cartesian expansions - a fast method for computing of potential of the form r - v for all real v," *J. Comput. Phys.*, vol. 226, pp. 732-753, Jan. 2007.

[9] M. Vikram, H. Huang, B. Shanker, and T. Van, "A novel wideband FMM for fast integral equation solution of multiscale problems in electromagnetics," *IEEE Trans. Antennas Propag.*, vol. 57, pp. 2094-2104, July 2009.

[10] Z. G. Qian and W. C. Chew, "Fast full-wave surface integral equation solver for multiscale structure modeling," *IEEE Trans. Antennas Propag.*, vol. 57, pp. 3594-3601, Nov. 2009.

[11] Z. G. Qian and W. C. Chew, "A quantitative study on the low-frequency breakdown of EFIE," *Micro. Opt. Technol. Lett.*, vol. 50. pp. 1159-1162, May 2008.

[12] J. S. Zhao and W. C. Chew, "Integral equation solution of Maxwell's equations from zero frequency to microwave frequencies," *IEEE Trans. Antennas Propagat.*, vol. 48, pp. 1635-1645, Oct. 2000.

[13] M. Taskinen and P. Ylä-Oijala, "Current and charge integral equation formulation," *IEEE Trans. Antennas Propagat.*, vol. 54, pp. 58-67, Jan. 2006.

[14] D. Gope, A. R. Ruehli, and V. Jandhyala, "Solving low-frequency EM-CKT problems using the PEEC method," *IEEE Trans. Adv. Packag.*, vol. 30, pp. 313-320, May 2007.

[15] Z. G. Qian and W. C. Chew, "Enhanced A-EFIE with perturbation method," *IEEE Trans. Antennas Propag.*, vol. 58, pp. 3256-3264, Dec. 2010

[16] J. Cheng and R. J. Adams, "Electric field-based surface integral constraints for Helmholtz decompositions of the current on a conductor,"

IEEE Trans. Antennas Propag., vol. 61, pp. 4632-4640, Sep. 2013.

[17] N. Hendijani, J. Cheng, and R. J. Adams, "Combined field integral equation using a constraint-based Helmholtz decomposition," *IEEE Trans. Antennas Propag.*, vol. 62, pp. 1500-1503, Mar. 2014.

scattering. He has received the second prize of the National Award for Science and Technology Progress.

Zaiping Nie was born in Xi`an, China, in 1946. He received the B.S. degree in Radio Engineering and the M.S. degree in Electro-magnetic Field and Microwave Technology from the Chengdu Institute of Radio Engineering (now UESTC: University of Electronic Science and Technology of China), Chengdu, P. R. China, in 1968 and 1981, respectively. From 1987 to 1989, he was a Visiting Scholar with the Electromagnetics Laboratory, University of Illinois, Urbana. Currently, he is a Professor with the Department of Microwave Engineering, UESTC. Nie is a Fellow of IEEE. He has published more than 300 journal papers. His research interests include antenna theory and techniques, fields and waves in inhomogeneous media, computational electromagnetics, electromagnetic scattering and inverse scattering, new techniques for antenna in mobile communications, and transient electromagnetic theory and applications.

Yuteng Zheng was born in Lanzhou, China, in 1988. He received the B.S. degree in Electromagnetics and Microwave Technology from the University of Electronic Science and Technology of China, Chengdu, in 2010, where he is currently working toward his Ph.D. degree. His research interests include numerical methods in computational electromagnetics, especially integral equation based methods and fast algorithms.

Yanwen Zhao was born in Sichuan Province of China, March 23, 1965. He received the M.S. degree in Geophysical Exploration from the University of Chang Jiang in 1994, and the Ph.D. degree in Electrical Engineering from the University of Electrical and Science Technology of China (UESTC). He is currently a Professor of Electrical Engineering in UESTC. Zhao is a Senior Member of the Chinese Institute of Electronics. His research interests include computational electromagnetics, fields and waves in inhomogeneous media and inverse

Qiangming Cai was born in Sichuan Province of China, on December 12, 1987. He received the B.S. degree in Physics from the Sichuan Normal University, China, in 2011, and is currently working toward the Ph.D. degree in the University of Electrical and Science Technology of China (UESTC). His research interests include numerical methods in electromagnetics with focus on fast solution of frequency domain integral equation.